

# 1 Theory of Linear Response in a Nutshell

This section summarizes some important derivations from [Vonsovskii and Katsnel'son, 1989] and [Giuliani and Vignale, 2005] that are crucial for further calculations.

**Classically** Consider an electron system subject to small external perturbation  $V_{\text{ext}}(\mathbf{r}, t)$ . By definition of the *inverse dielectric function* the total potential  $V(\mathbf{r}, t)$  is given by

$$V(\mathbf{r}, t) = \int d^3 r' \int_{-\infty}^t dt' \varepsilon^{-1}(\mathbf{r}, \mathbf{r}', t - t') V_{\text{ext}}(\mathbf{r}', t') . \quad (1)$$

The upper bound of the integral over  $t'$  is  $t$  in place of  $\infty$  due to causality: the “effect” cannot precede the “cause”. This is equivalent to saying that  $\varepsilon^{-1}(\mathbf{r}, \mathbf{r}', \tau) = 0$  whenever  $\tau < 0$ . The Fourier transform of  $\varepsilon^{-1}(\mathbf{r}, \mathbf{r}', \tau)$  is

$$\varepsilon^{-1}(\mathbf{r}, \mathbf{r}', \omega) = \int_0^\infty d\tau e^{i\omega\tau} \varepsilon^{-1}(\mathbf{r}, \mathbf{r}', \tau) . \quad (2)$$

Applying Titchmarsh's theorem to  $\varepsilon^{-1}$ , we get that  $\varepsilon^{-1}(\mathbf{r}, \mathbf{r}', \omega)$  is the limit  $\eta \rightarrow 0+$  of  $\varepsilon^{-1}(\mathbf{r}, \mathbf{r}', \omega + i\eta)$  which is holomorphic in the upper complex plane. Taking Fourier transform of eq. (1), we obtain<sup>1</sup>

$$V(\mathbf{r}, \omega) = \int d^3 r' \varepsilon^{-1}(\mathbf{r}, \mathbf{r}', \omega) V_{\text{ext}}(\mathbf{r}', \omega) . \quad (3)$$

Eqs. (2) and (3) may equivalently be formulated as

$$\begin{aligned} V_{\text{ext}}(\mathbf{r}, \omega) &= \int d^3 r' \varepsilon(\mathbf{r}, \mathbf{r}', \omega) V(\mathbf{r}') , \text{ where} \\ \varepsilon(\mathbf{r}, \mathbf{r}', \omega) &= \lim_{\eta \rightarrow 0+} \varepsilon(\mathbf{r}, \mathbf{r}', \omega + i\eta) = \lim_{\eta \rightarrow 0+} \int_0^\infty d\tau e^{i(\omega+i\eta)\tau} \varepsilon(\mathbf{r}, \mathbf{r}', \tau) . \end{aligned} \quad (4)$$

<sup>1</sup>

$$\begin{aligned} V(\mathbf{r}, \omega) &= \int_{-\infty}^\infty dt e^{i\omega t} V(\mathbf{r}, t) \\ &= \int d^3 r' \int_{-\infty}^\infty dt \int_{-\infty}^t dt' e^{i\omega t} \varepsilon^{-1}(\mathbf{r}, \mathbf{r}', t - t') V_{\text{ext}}(\mathbf{r}', t') \\ &= \int d^3 r' \int_{-\infty}^\infty \frac{d\omega'}{2\pi} \int_{-\infty}^\infty dt \int_{-\infty}^t dt' e^{i\omega t} e^{-i\omega' t'} \varepsilon^{-1}(\mathbf{r}, \mathbf{r}', t - t') V_{\text{ext}}(\mathbf{r}', \omega') \\ &= \int d^3 r' \int_{-\infty}^\infty \frac{d\omega'}{2\pi} V_{\text{ext}}(\mathbf{r}', \omega') \int_{-\infty}^\infty dt \int_{-\infty}^t dt' e^{i(\omega-\omega')t} e^{i\omega'(t-t')} \varepsilon^{-1}(\mathbf{r}, \mathbf{r}', t - t') \\ &= \int d^3 r' \int_{-\infty}^\infty \frac{d\omega'}{2\pi} V_{\text{ext}}(\mathbf{r}', \omega') \int_{-\infty}^\infty dt e^{i(\omega-\omega')t} \int_{\infty}^0 (-d\tau) e^{i\omega'\tau} \varepsilon^{-1}(\mathbf{r}, \mathbf{r}', \tau) \\ &= \int d^3 r' \int_{-\infty}^\infty d\omega' \varepsilon^{-1}(\mathbf{r}, \mathbf{r}', \omega') V_{\text{ext}}(\mathbf{r}', \omega') \cdot \frac{1}{2\pi} \int_{-\infty}^\infty dt e^{i(\omega-\omega')t} \\ &= \int d^3 r' \varepsilon^{-1}(\mathbf{r}, \mathbf{r}', \omega) V_{\text{ext}}(\mathbf{r}', \omega) . \end{aligned}$$

**Quantum Mechanically** Now consider a system of non-interacting electrons described in a single-particle approximation by a Hamiltonian  $\hat{H}_0$ . Let  $E_i$  denote single-particle energy levels with corresponding eigenstates  $|i\rangle$ . One-particle density matrix is then

$$\hat{\rho}_0 = \sum_i n_i |i\rangle\langle i| , \quad (5)$$

where  $n_i$  denotes the occupational number at energy  $E_i$  which, in equilibrium, is given by the Fermi-Dirac distribution. Electron density operator is  $\hat{N}(\mathbf{r}) = |\mathbf{r}\rangle\langle\mathbf{r}|$ . Equation of motion reads

$$i\hbar \frac{d\hat{\rho}_0}{dt} = [\hat{H}_0, \hat{\rho}_0] = 0 .$$

Within RPA (Random Phase Approximation) we are interested in the reponse of the system to the perturbation of the form  $\hat{V}e^{-i(\omega+i\eta)t}$ <sup>2</sup>. In the first order approximation,  $\hat{\rho} = \hat{\rho}_0 + \hat{\rho}' + \mathcal{O}(\hat{V}^2)$ , where  $\hat{\rho}_0$  is defined by eq. (5) and  $\hat{\rho}' \propto \hat{V}$ . We thus have

$$\left. \begin{aligned} i\hbar \frac{d\hat{\rho}}{dt} &= i\hbar \frac{d\hat{\rho}_0}{dt} + i\hbar \frac{d\hat{\rho}'}{dt} \\ [\hat{H}, \hat{\rho}] &= [\hat{H}_0, \hat{\rho}_0] + [\hat{H}_0, \hat{\rho}'] + [\hat{V}, \hat{\rho}_0]e^{-i(\omega+i\eta)t} + \mathcal{O}(\hat{V}^2) \end{aligned} \right\} \implies i\hbar \frac{d\hat{\rho}'}{dt} = [\hat{H}_0, \hat{\rho}'] + [\hat{V}, \hat{\rho}_0]e^{-i(\omega+i\eta)t} . \quad (6)$$

Using an ansatz  $\hat{\rho}' = \tilde{G}\hat{V}e^{-i(\omega+i\eta)t}$ , where  $\tilde{G}$  is some time-independent operator, we obtain<sup>3</sup>

$$\begin{aligned} \langle i|\tilde{G}\hat{V}|j\rangle &= \frac{n_i - n_j}{E_i - E_j - \hbar(\omega + i\eta)} \langle i|\hat{V}|j\rangle \\ &\equiv \langle i|\hat{G}|j\rangle \langle i|\hat{V}|j\rangle , \end{aligned}$$

where we have defined a new operator  $\hat{G}$  by

$$\langle i|\hat{G}|j\rangle = \frac{n_i - n_j}{E_i - E_j - \hbar(\omega + i\eta)} . \quad (7)$$

We can now calculate the induced electron density  $\delta\hat{N}(t)$ :

$$\begin{aligned} \langle \mathbf{r}|\delta\hat{N}(t)|\mathbf{r}\rangle &= \text{Tr}(\hat{N}(\mathbf{r})\hat{\rho}) - \text{Tr}(\hat{N}(\mathbf{r})\hat{\rho}_0) = \text{Tr}(\hat{N}(\mathbf{r})\hat{\rho}') \\ &= \sum_{i,j} \langle j|\mathbf{r}\rangle\langle\mathbf{r}|i\rangle \langle i|\tilde{G}\hat{V}|j\rangle e^{-i(\omega+i\eta)t} \\ &= \sum_{i,j} \langle i|\hat{G}|j\rangle \langle j|\mathbf{r}\rangle\langle\mathbf{r}|i\rangle \langle i|\hat{V}|j\rangle e^{-i(\omega+i\eta)t} . \end{aligned} \quad (8)$$

---

<sup>2</sup>Notice the appearance of  $\eta$ . It may be viewed either mathematically, as trick to be able to use eq. 4, or physically, as an adiabatic turning on of the potential. For further discussion of the significance of this factor, see [Nussenzveig, 1972]

<sup>3</sup>Calculating matrix elements:

$$\begin{aligned} \langle i|i\hbar \frac{d\hat{\rho}'}{dt}|j\rangle &= \hbar(\omega + i\eta)\langle i|\hat{\rho}'|j\rangle , \\ \langle i|[\hat{H}_0, \hat{\rho}']|j\rangle &= (E_i - E_j)\langle i|\hat{\rho}'|j\rangle , \\ \langle i|[\hat{V}, \hat{\rho}_0]|j\rangle &= (n_j - n_i)\langle i|\hat{V}|j\rangle . \end{aligned}$$

Eq. (6) now reads

$$\langle i|\hat{\rho}'|j\rangle = \frac{(n_i - n_j)e^{-i\omega t + i\eta t}}{E_i - E_j - \hbar(\omega + i\eta)} \langle i|\hat{V}|j\rangle .$$

The total potential  $\hat{V}$  is the sum of external potential  $\hat{V}_{\text{ext}}$  and the potential induced by the variation of the charge density, i.e.

$$\langle \mathbf{r} | \hat{V}_{\text{tot}}(t) | \mathbf{r} \rangle = \langle \mathbf{r} | \hat{V}_{\text{ext}}(t) | \mathbf{r} \rangle + \int d^3 r' \langle \mathbf{r} | \hat{V}_{\text{Coulomb}} | \mathbf{r}' \rangle \langle \mathbf{r}' | \delta \hat{N}(t) | \mathbf{r}' \rangle , \quad (9)$$

where  $\hat{V}_{\text{Coulomb}}$  is the Coulomb interaction potential. We have also used the fact that  $\hat{V}$  is diagonal in position representation. Using eq. (8) we get<sup>4</sup>

$$\begin{aligned} \langle \mathbf{r} | \hat{V}_{\text{ext}}(t) | \mathbf{r} \rangle &= \int d^3 r' \langle \mathbf{r} | \hat{\varepsilon}(t) | \mathbf{r}' \rangle \langle \mathbf{r}' | \hat{V} | \mathbf{r}' \rangle , \text{ where} \\ \langle \mathbf{r} | \hat{\varepsilon}(\tau) | \mathbf{r}' \rangle &= \left( \langle \mathbf{r} | \mathbf{r}' \rangle - \sum_{i,j} \langle i | \hat{G} | j \rangle \int d^3 r'' \frac{e^2}{\| \mathbf{r} - \mathbf{r}'' \|} \langle j | \mathbf{r}'' \rangle \langle \mathbf{r}'' | i \rangle \langle i | \mathbf{r}' \rangle \langle \mathbf{r}' | j \rangle \right) e^{-i(\omega+i\eta)\tau} . \end{aligned}$$

Using Titchmarsh's theorem once again, we obtain

$$\begin{aligned} \langle \mathbf{r} | \hat{V}_{\text{ext}}(\omega) | \mathbf{r} \rangle &= \int d^3 r' \langle \mathbf{r} | \hat{\varepsilon}(\omega) | \mathbf{r}' \rangle \langle \mathbf{r}' | \hat{V} | \mathbf{r}' \rangle , \text{ where} \\ \langle \mathbf{r} | \hat{\varepsilon}(\omega) | \mathbf{r}' \rangle &= \lim_{\eta \rightarrow 0+} \langle \mathbf{r} | \hat{\varepsilon}(\omega + i\eta) | \mathbf{r}' \rangle = \lim_{\eta \rightarrow 0+} \int_0^\infty d\tau e^{i(\omega+i\eta)\tau} \langle \mathbf{r} | \varepsilon(\tau) | \mathbf{r}' \rangle \\ &= \langle \mathbf{r} | \mathbf{r}' \rangle - \lim_{\eta \rightarrow 0+} \sum_{i,j} \langle i | \hat{G} | j \rangle \int d^3 r'' \frac{e^2}{\| \mathbf{r} - \mathbf{r}'' \|} \langle j | \mathbf{r}'' \rangle \langle \mathbf{r}'' | i \rangle \langle i | \mathbf{r}' \rangle \langle \mathbf{r}' | j \rangle \quad (10) \\ &= \langle \mathbf{r} | \mathbf{r}' \rangle - \int d^3 r'' \langle \mathbf{r} | \hat{V}_{\text{Coulomb}} | \mathbf{r}'' \rangle \langle \mathbf{r}'' | \hat{\chi}(\omega) | \mathbf{r}' \rangle , \\ \langle \mathbf{r}'' | \hat{\chi}(\omega) | \mathbf{r}' \rangle &= \lim_{\eta \rightarrow 0+} \sum_{i,j} \langle i | \hat{G} | j \rangle \langle j | \mathbf{r}'' \rangle \langle \mathbf{r}'' | i \rangle \langle i | \mathbf{r}' \rangle \langle \mathbf{r}' | j \rangle , \\ \langle \mathbf{r} | \hat{V}_{\text{Coulomb}} | \mathbf{r}'' \rangle &= \frac{e^2}{\| \mathbf{r} - \mathbf{r}'' \|} , \end{aligned}$$

which is the exact equivalent of eq. (4) in the classical description.  $\hat{\chi}$  is called the *polarizability matrix*.

---

<sup>4</sup>At point  $\mathbf{r}$  we have

$$\begin{aligned} \langle \mathbf{r} | \hat{V}_{\text{ext}}(t) | \mathbf{r} \rangle &= \langle \mathbf{r} | \hat{V}_{\text{tot}}(t) | \mathbf{r} \rangle - \int d^3 r' \frac{e^2}{\| \mathbf{r} - \mathbf{r}' \|} \langle \mathbf{r}' | \delta \hat{N}(t) | \mathbf{r}' \rangle \\ &\stackrel{(8)}{=} \langle \mathbf{r} | \hat{V} | \mathbf{r} \rangle e^{-i(\omega+i\eta)t} - \int d^3 r' \frac{e^2}{\| \mathbf{r} - \mathbf{r}' \|} \sum_{i,j} \langle i | \hat{G} | j \rangle e^{-i(\omega+i\eta)t} \langle j | \mathbf{r}' \rangle \langle \mathbf{r}' | i \rangle \langle i | \hat{V} | j \rangle \\ &= \left( \langle \mathbf{r} | \hat{V} | \mathbf{r} \rangle - \sum_{i,j} \langle i | \hat{G} | j \rangle \int d^3 r' \int d^3 r'' \int d^3 r''' \frac{e^2}{\| \mathbf{r} - \mathbf{r}' \|} \langle j | \mathbf{r}' \rangle \langle \mathbf{r}' | i \rangle \langle i | \mathbf{r}'' \rangle \langle \mathbf{r}''' | j \rangle \langle \mathbf{r}''' | \hat{V} | \mathbf{r}''' \rangle \right) e^{-i(\omega+i\eta)t} \\ &= \left( \langle \mathbf{r} | \hat{V} | \mathbf{r} \rangle - \sum_{i,j} \langle i | \hat{G} | j \rangle \int d^3 r' \int d^3 r'' \frac{e^2}{\| \mathbf{r} - \mathbf{r}' \|} \langle j | \mathbf{r}' \rangle \langle \mathbf{r}' | i \rangle \langle i | \mathbf{r}'' \rangle \langle \mathbf{r}'' | j \rangle \langle \mathbf{r}'' | \hat{V} | \mathbf{r}'' \rangle \right) e^{-i(\omega+i\eta)t} . \end{aligned}$$

## 2 Application

We now apply the results of sec. 1 to a finite 2D lattice described in the tight binding approximation. We do the calculation in *atomic basis*, i.e. the basis of local site wave functions  $|a\rangle$  ( $a \in \{0, N - 1\}$ , where  $N$  is the number of sites). The following assumptions are made:

- $\langle a|b\rangle = \delta_{a,b}$ ,
- atomic basis is complete, i.e.  $\sum_a |a\rangle\langle a| = \hat{\mathbb{1}}$ ,
- $|a\rangle$ 's are localized around the corresponding sites, i.e.  $\langle \mathbf{r}|a\rangle \approx \delta(\mathbf{r} - \mathbf{r}_a)$ , where  $\mathbf{r}_a$  is the position of  $a$ 'th site. This is the key to making a step from analytical formulas to numerical calculations.

These assumptions essentially mean that the step from position representation to atomic basis is performed by  $|\mathbf{r}\rangle \rightarrow |a\rangle$ ,  $\mathbf{r} \rightarrow \mathbf{r}_a$  and  $\int d^3r \rightarrow \sum_a$ . Another important step is to replace  $\hat{G}$  by  $2\hat{G}$ . Now  $i$  and  $j$  indices also run from 0 to  $N - 1$ . Eq. (10) now reads<sup>5</sup>

$$\begin{aligned} \langle a|\hat{V}_{\text{ext}}(\omega)|a\rangle &= \sum_b \langle a|\hat{\varepsilon}(\omega)|b\rangle\langle b|\hat{V}|b\rangle, \text{ where} \\ \langle a|\hat{\varepsilon}(\omega)|b\rangle &= \langle a|b\rangle - \sum_c \langle a|\hat{V}_{\text{Coulomb}}|c\rangle\langle c|\hat{\chi}(\omega)|b\rangle, \\ \langle a|\hat{\chi}(\omega)|b\rangle &= 2 \cdot \lim_{\eta \rightarrow 0+} \sum_{i,j} \langle i|\hat{G}|j\rangle\langle j|a\rangle\langle a|i\rangle\langle i|b\rangle\langle b|j\rangle, \\ \langle a|\hat{V}_{\text{Coulomb}}|b\rangle &= \begin{cases} \frac{1}{4\pi\epsilon_0} \frac{e}{\|\mathbf{r}_a - \mathbf{r}_b\|} & , \text{ if } a \neq b, \\ V_0 & , \text{ if } a = b, \end{cases} \end{aligned} \quad (11)$$

The trick that allows the calculations of  $\hat{\chi}(\omega)$  in a reasonable time is to rewrite it in terms of matrices:

$$\begin{aligned} \langle a|\hat{\chi}(\omega)|b\rangle &= \underbrace{A(a,b)}_{\substack{\text{row vector} \\ \text{square matrix}}} \underbrace{\hat{G}}_{\substack{\text{column vector} \\ \text{square matrix}}} \underbrace{A(a,b)^\dagger}_{\substack{\text{column vector} \\ \text{square matrix}}} = \underbrace{\left( \underbrace{\hat{G}^T A(a,b)^T}_{\text{GEMV}} \right)^T}_{\text{DOT}} A(a,b)^\dagger, \text{ where} \\ G_{i,j} &= \langle i|\hat{G}|j\rangle \stackrel{(7)}{=} \frac{n_i - n_j}{E_i - E_j - \hbar(\omega + i\eta)} \quad \text{with } \eta \text{ small, and} \\ A(a,b)_i &= \langle a|i\rangle\langle i|b\rangle = \langle a|i\rangle\langle b|i\rangle^*. \end{aligned} \quad (12)$$

The second form of  $\langle a|\hat{\chi}(\omega)|b\rangle$  with a lot of transposes may seem strange, but it is of utmost importance. It allows us to calculate matrix elements of  $\hat{\chi}(\omega)$  using just two BLAS operations: matrix-vector product (GEMV) and dot-product (DOT). It is now straightforward to write a highly parallel implementation of eq. (12) and it will not be discussed here any further.

With eqs. (11) and (12) implemented, we can obtain  $\hat{\varepsilon}(\omega)$  for any system, given its tight-binding Hamiltonian  $\hat{H}$  and sites positions  $\{\mathbf{r}_a | a \in \{0, \dots, N - 1\}\}$ . We thus, in principle, have complete knowledge of the optical properties of the system.

---

<sup>5</sup>Eq. (10) was written in Gauss system. For the calculations it is, however, easier to use electron-volts. We thus replace  $e^2$  by  $\frac{e}{4\pi\epsilon_0}$ . We also introduce the *self-interaction potential*  $V_0$  to prevent degeneracies in  $\langle a|\hat{V}_{\text{Coulomb}}|a\rangle$ .

### 3 Experiments

Let's now apply the acquired tools to examine plasmonic properties of some systems. For this we need a way of visualising the results. The most common way to measure plasmonic properties is through EELS (*Electron Energy Loss Spectroscopy*) experiments. We are not going to discuss these experiments in detail here. But the basic idea is to shoot electrons with well defined wavevector  $\mathbf{q}$  on the sample. The double differential cross section  $d^2\sigma/d\Omega dE$  (with  $\Omega$  — solid angle,  $E$  — energy lost during collision) is proportional to the *loss function* —  $\text{Im}[1/\langle \mathbf{q} | \hat{\epsilon}(\omega) | \mathbf{q} \rangle]$ . The QM derivation is rather technical and will not be given here. [Jackson, 1925] gives a good classical description. An in-depth explanation of EELS experiments may be found in [Egerton, 2009].

An interesting approach to calculating the loss spectrum is provided in [Wang Weihua et al., 2015]. It goes as follows. Consider the classical definition of a plasmon:  $\epsilon(\omega) = 0$ . In reality, there is also loss due to the parameter  $\eta \neq 0$  in eq. (11). We then consider the spectral representation of the dielectric function<sup>6</sup>

$$\hat{\epsilon}(\omega) = \sum_n \epsilon_n(\omega) |\phi_n(\omega)\rangle\langle\phi_n(\omega)|.$$

Plasmons frequencies are then identified by eigenvalues of  $\hat{\epsilon}$  with zero real part:

$$\hat{\epsilon}(\omega)|\phi_n(\omega)\rangle = \epsilon_n(\omega)|\phi_n(\omega)\rangle, \text{ such that } \epsilon_n(\omega) \in \mathbb{C} \setminus \mathbb{R}, \text{ i.e. purely imaginary.} \quad (13)$$

As noted in [Andersen et al., 2012], “when the imaginary part of eigenvalue  $\epsilon_n(\omega)$  does not vary too much around the plasmon frequency  $\omega'$ ”, condition (13) is equivalent to the condition that

$$-\text{Im}[\epsilon_n^{-1}(\omega)] \text{ has a local maximum at } \omega'. \quad (14)$$

In [Wang Weihua et al., 2015] the *loss function* is defined as  $-\text{Im}[\epsilon_{n(\omega)}^{-1}(\omega)]$ , where  $n(\omega)$  is the index of the eigenvalue with the highest  $-\text{Im}[\epsilon_j^{-1}(\omega)]$ . This provides a “real space analogue” of  $-\text{Im}[1/\langle \mathbf{q} | \hat{\epsilon}(\omega) | \mathbf{q} \rangle]$ . The most appealing part in this approach is the fact that we can easily get insight into the spatial form of plasmon eigenmodes. For a certain frequency  $\omega$   $\text{Re}[\langle \mathbf{r} | \phi_{n(\omega)} \rangle]$  shows how the eigenstate looks like. [Andersen et al., 2012] show that  $|\phi_{n(\omega)}\rangle$ 's correspond to plasmon (**TODO**: density or potential??) eigenstates.

Another approach is to just calculate  $\langle \mathbf{q} | \hat{\epsilon}(\omega) | \mathbf{q} \rangle$ . In the tight binding model we can effi-

---

<sup>6</sup>Here, we implicitly assumed that the dielectric function  $\hat{\epsilon}(\omega)$  is diagonalizable. This is not true in general. For a real Hamiltonian, however, both eigenvalues and eigenstates are real. Then from eq. (11) it follows that the dielectric function is also symmetric, i.e.  $\langle a | \hat{\epsilon}(\omega) | b \rangle = \langle b | \hat{\epsilon}(\omega) | a \rangle$ . Now, obviously, a symmetric matrix is diagonalizable.

Hence, the approach of [Wang Weihua et al., 2015] is only valid for real Hamiltonians.

ciently calculate it as<sup>7</sup>

$$\begin{aligned}
\langle \mathbf{q} | \hat{\varepsilon}(\omega) | \mathbf{q} \rangle &= \sum_{a,b} \langle \mathbf{q} | a \rangle \overbrace{\langle a | \hat{\varepsilon}(\omega) | b \rangle}^{\text{matrix } A} \underbrace{\langle b | \mathbf{q} \rangle}_{\text{vector } v} \\
&= v^\dagger A v = (v^\dagger A v)^T = v^T A^T v^* = v^T (A^\dagger v)^* \\
&= \underbrace{(A^\dagger v)^\dagger v}_{\substack{\text{GEMV} \\ \text{CDOT}}} .
\end{aligned}$$

The advantage of this approach is its direct correspondence to EELS experiments.

Yet another way to couple  $\hat{\varepsilon}(\omega)$  to experiments is to calculate the induced charge density. From eq. (10), we get<sup>8</sup>

$$\langle \mathbf{r} | \hat{V} | \mathbf{r} \rangle = \int d^3 r' \langle \mathbf{r} | \hat{\varepsilon}^{-1}(\omega) | \mathbf{r}' \rangle \langle \mathbf{r}' | \hat{V}_{\text{ext}}(\omega) | \mathbf{r}' \rangle .$$

We can now insert this result into eq. (9) to obtain

$$\langle \mathbf{r} | \delta \hat{N}(\omega) | \mathbf{r} \rangle = \int d^3 r'' \langle \mathbf{r} | \hat{V}_{\text{Coulomb}}^{-1} | \mathbf{r}'' \rangle \cdot \left( \int d^3 r' \langle \mathbf{r}'' | \hat{\varepsilon}^{-1}(\omega) | \mathbf{r}' \rangle \langle \mathbf{r}' | \hat{V}_{\text{ext}}(\omega) | \mathbf{r}' \rangle - \langle \mathbf{r}'' | \hat{V}_{\text{ext}}(\omega) | \mathbf{r}'' \rangle \right) . \quad (15)$$

This allows one to study the effects of different external potentials on the charge density in the sample. There is, however, no simple way to tell whether a certain charge density distribution corresponds to a plasmon.

Having discussed the relation of  $\hat{\varepsilon}(\omega)$  to experiments, we go on and calculate some of these measurable quantities for different systems.

---

<sup>7</sup>

$$\begin{aligned}
\langle \mathbf{q} | \hat{\varepsilon}(\omega) | \mathbf{q} \rangle &= \int d^3 r \int d^3 r' \langle \mathbf{q} | \mathbf{r} \rangle \langle \mathbf{r} | \hat{\varepsilon}(\omega) | \mathbf{r}' \rangle \langle \mathbf{r}' | \mathbf{q} \rangle \\
&= \int d^3 r \int d^3 r' \langle \mathbf{q} | \mathbf{r} \rangle \langle \mathbf{r} | \hat{\varepsilon}(\omega) | \mathbf{r}' \rangle \langle \mathbf{r}' | \mathbf{q} \rangle \\
&= \frac{1}{(2\pi)^3} \int d^3 r \int d^3 r' \langle \mathbf{r} | \hat{\varepsilon}(\omega) | \mathbf{r}' \rangle e^{-i\mathbf{q}(\mathbf{r}-\mathbf{r}')} .
\end{aligned}$$

<sup>8</sup>

$$\begin{aligned}
\langle \mathbf{r} | \hat{V}_{\text{ext}}(\omega) | \mathbf{r} \rangle &= \int d^3 r' \langle \mathbf{r} | \hat{\varepsilon}(\omega) | \mathbf{r}' \rangle \langle \mathbf{r}' | \hat{V} | \mathbf{r}' \rangle \\
\int d^3 r \langle \mathbf{r}'' | \hat{\varepsilon}^{-1}(\omega) | \mathbf{r} \rangle \langle \mathbf{r} | \hat{V}_{\text{ext}}(\omega) | \mathbf{r} \rangle &= \int d^3 r' \int d^3 r \langle \mathbf{r}'' | \hat{\varepsilon}^{-1}(\omega) | \mathbf{r} \rangle \langle \mathbf{r} | \hat{\varepsilon}(\omega) | \mathbf{r}' \rangle \langle \mathbf{r}' | \hat{V} | \mathbf{r}' \rangle \\
\int d^3 r \langle \mathbf{r}'' | \hat{\varepsilon}^{-1}(\omega) | \mathbf{r} \rangle \langle \mathbf{r} | \hat{V}_{\text{ext}}(\omega) | \mathbf{r} \rangle &= \int d^3 r' \langle \mathbf{r}'' | \mathbf{r}' \rangle \langle \mathbf{r}' | \hat{V} | \mathbf{r}' \rangle \\
\int d^3 r \langle \mathbf{r}'' | \hat{\varepsilon}^{-1}(\omega) | \mathbf{r} \rangle \langle \mathbf{r} | \hat{V}_{\text{ext}}(\omega) | \mathbf{r} \rangle &= \langle \mathbf{r}'' | \hat{V} | \mathbf{r}'' \rangle
\end{aligned}$$

### 3.1 Graphene nanotriangles

We start with a toy system — a small graphene nanotriangle. Picture ?? shows the system. Although it is approximately two times smaller than the triangles used in [Wang Weihua et al., 2015], it is big enough for testing purposes. Our implementation of eq. (11) significantly differs from the one used in [Wang Weihua et al., 2015]. It thus seems like a good check to see whether our implementation produces the same results.

Using TIPSI Python package we can construct the tight-binding Hamiltonian for the problem. Hopping value of 2.8 eV is used. All other parameters like the chemical potential  $\mu = 0.4$  eV, temperature  $T = 300$  K, and “inverse relaxation time”  $\eta = 6$  meV/ $\hbar$  are also taken to be the same as in [Wang Weihua et al., 2015].

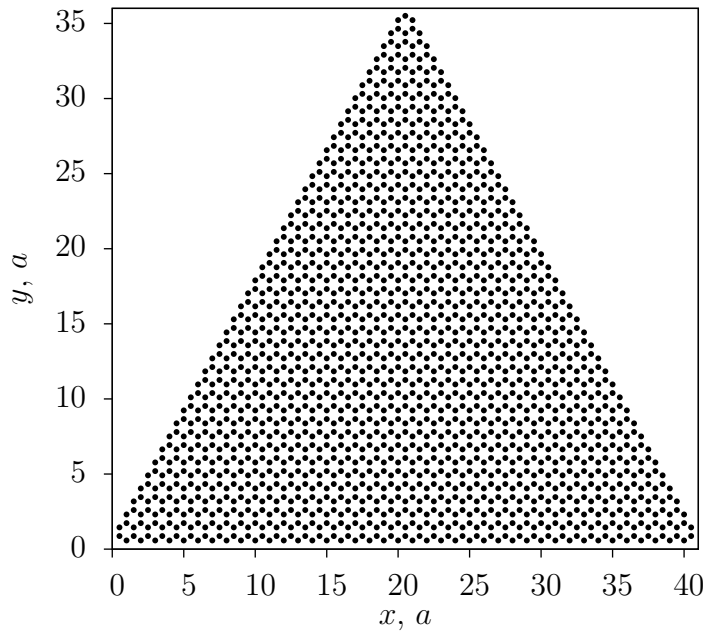


Figure 1: Graphene nanotriangle with zigzag edges. It has a width of  $40 \cdot a \approx 10$  nm.

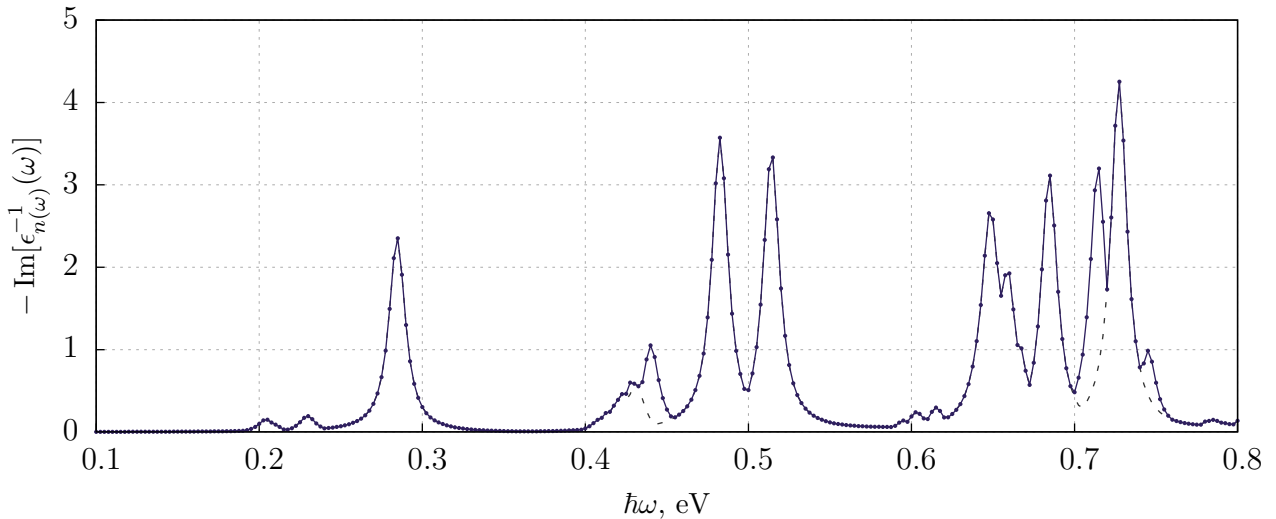


Figure 2: Low-energy loss spectrum for a zigzag-edged graphene nanotriangle.

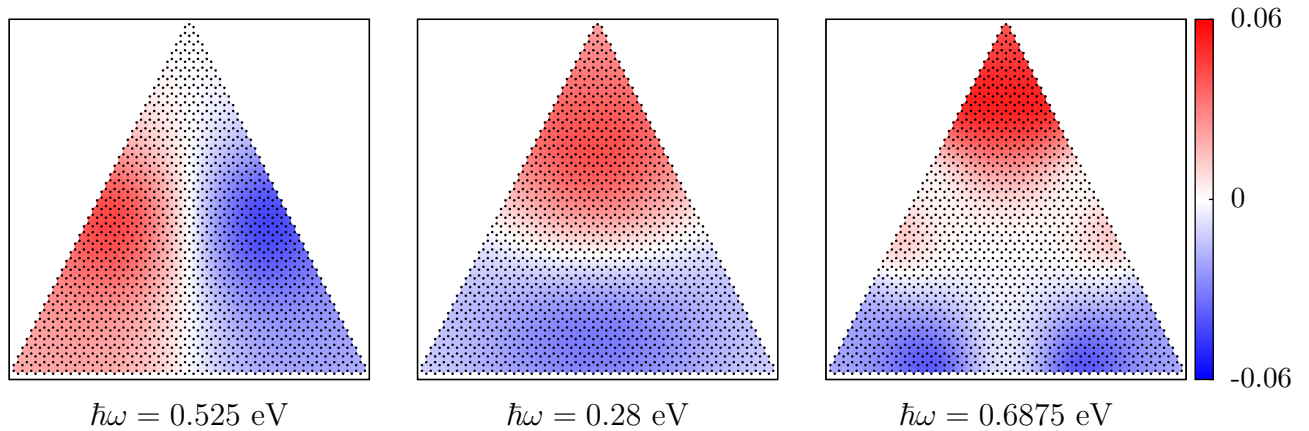


Figure 3: Some of the plasmon eigenmodes. These eigenmodes were also found by [Wang Weihua et al., 2015].

We calculated dielectric function for frequencies corresponding to  $\hbar\omega \in [0.1, 0.8]$  eV. Resulting loss spectrum, i.e.  $-\text{Im}[\hat{\varepsilon}_{n(\omega)}^{-1}(\omega)]$  vs.  $\omega$  plot is shown on fig. ???. We also show a couple of eigenmodes on fig. ??.

We won't discuss the results much further because it has been done extensively in [Wang Weihua et al., 2015], but an important conclusion is that our code works!

### 3.2 Third iteration Sierpinski carpet

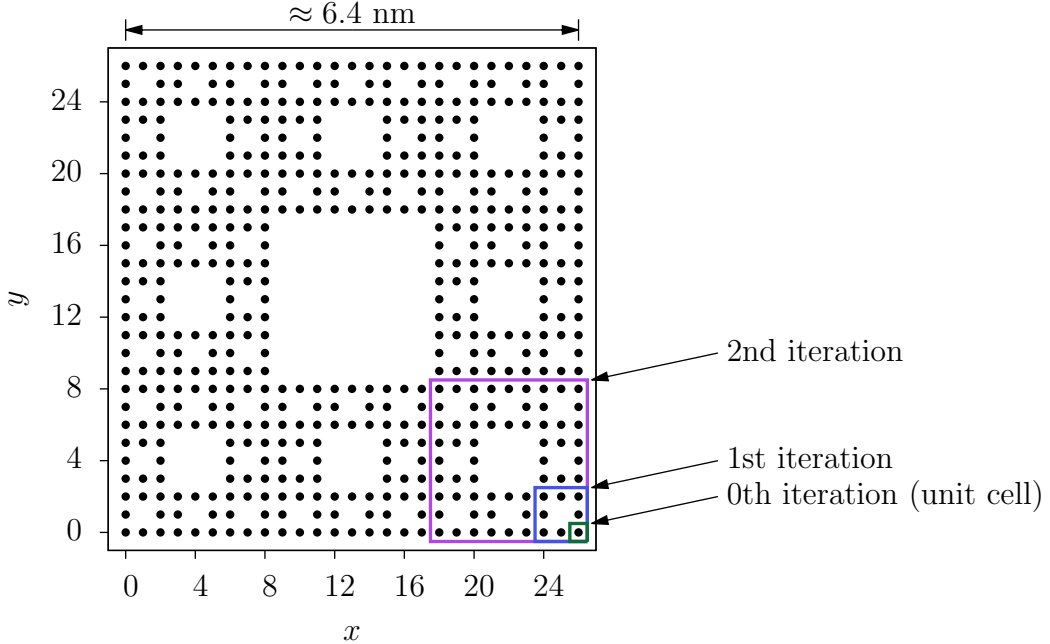


Figure 4: Third iteration Sierpinski carpet.  $x$  and  $y$  coordinates are given in terms of lattice constant. Width of the sample is  $3^3 = 27$  unit cells. In this case we chose the lattice constant of graphene  $a \approx 0.246$  nm, which results in the total width of about six and a half nanometers.

Next, we turn to somewhat smaller system — third iteration Siepinski carpet. The sample is shown in fig. 1. The Hamiltonian was, again, constructed using TIPSI, and we kept all the configuration parameters such as temperature and chemical potential the same. As we need eigenenergies and eigenstates anyway to make use of eq. (11), we can have a look at the density of states (fig. 2). Although the number of points is quite small (512 atomic sites), we can still extract some information.

For example, all possible energies lie within the  $(-9.5$  eV,  $9.5$  eV) range. Hence,  $E_i - E_j < 19$  eV for any  $i, j$ .  $G_{i,j}$  has  $(E_i - E_j - \hbar(\omega + i\eta))$  in the denominator, thus for  $\omega$ 's greater than  $\approx 20$  eV the loss function will asymptotically approach zero — no need to search for plasmons there.

To calculate the dielectric function, we need to choose a couple more parameters of the system. We chose the temperature of the system  $T$  be 300 K (i.e. room temperature). Chemical potential is taken to be  $\mu = 0.4$  eV, self-interaction coulomb potential —  $V_0 = 15.78$  eV, and the “inverse relaxation

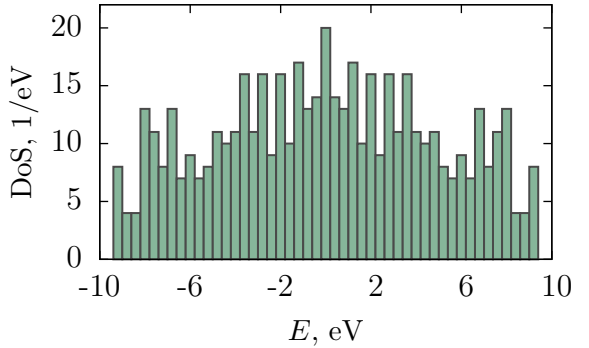


Figure 5: Density of states for the 3rd iteration SC. Due to the small size of the system, we can't say much about the distribution of energy eigenvalues (it has not yet converged).

time” —  $\hbar\eta = 0.006$  eV. These values are taken from [Wang Weihua et al., 2015]. Having chosen all configuration parameters we calculate  $\hat{\epsilon}(\omega)$  for frequencies up to  $\approx 22$  eV. All computations are performed on the **Cartesius** supercomputer in Amsterdam. For this, a highly parallel implementation of eq. (11) had been written. It is discussed in ??.

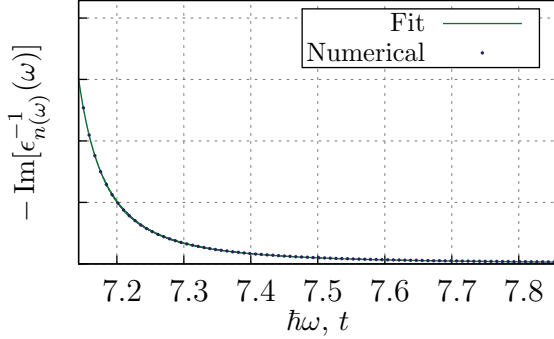


Figure 6: This plot shows asymptotic behavior of the loss function at high frequencies. Loss function (in arbitrary units) is plotted against electron energy loss (in  $t$ , hopping value). “Numerical” curve is the result of the precise numerical calculation. “Fit” is obtained by fitting  $a/((b - \omega)^2 + c^2)$  (i.e. eq. (16)) to the results of numerical calculations.

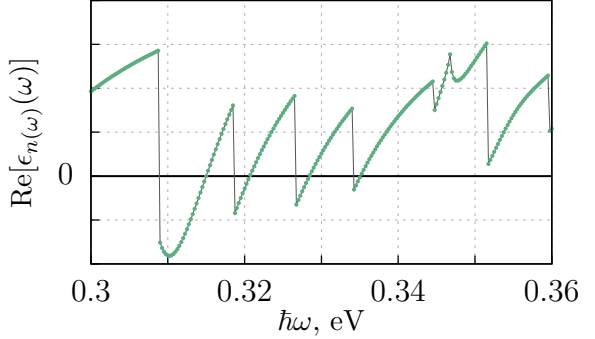


Figure 7: Behavior of  $\text{Re}[\epsilon_{n(\omega)}(\omega)]$  is shown. A really narrow interval of frequencies is chosen for clarity.

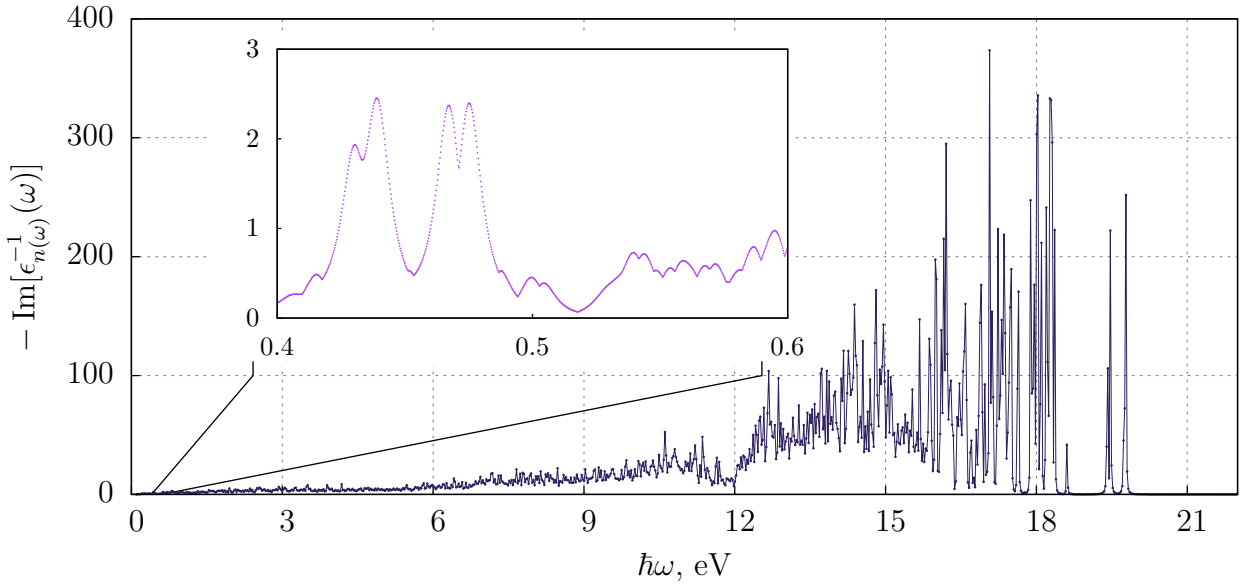


Figure 8: Loss function spectrum for the third iteration Sierpinski carpet.

First of all, let’s discuss the asymptotic behavior of the loss function at high frequencies. Let’s ignore for a minute the fact that  $\hat{\epsilon}(\omega)$  is a matrix. Using eq. (11) we can approximate it by

$$\epsilon(\omega) \approx 1 - \frac{A}{B - \omega + i \cdot C},$$

and the loss function becomes<sup>9</sup>

$$-\text{Im} \left[ \frac{1}{\epsilon(\omega)} \right] \approx \frac{a}{(b - \omega)^2 + c^2}, \text{ where } a = AC, \ b = B - A, \ c = C. \quad (16)$$

Fig. 3 shows how good this approximation actually is. This model describes the loss function very well for energies higher than  $\max_{i,j} |E_i - E_j|$ .

**r-approach** We first consider the loss function as defined in [Wang Weihua et al., 2015]. Spectrum for the full range of calculated frequencies is shown on fig. 5. With our definition of a plasmon, high number of sharp peaks means that there are plenty of plasmons. It is interesting to compare the classical definition of plasmon (i.e. condition (13)) to the condition that loss function has a local maximum. Fig. 4 shows the behavior of the real part of the dielectric function  $\epsilon_{n(\omega)}(\omega)$ . Although it is plotted for a very narrow range of energies, it exhibits the same behavior in general. We only identify the actual roots of  $\text{Re}[\epsilon_{n(\omega)}(\omega)]$  (not points of discontinuity) with plasmon frequencies. For this we focus on the infrared part of the spectrum in fig. 5 as low-energy plasmon modes are easier to excite experimentally. Fig. 6 shows the infrared part of the loss spectrum.

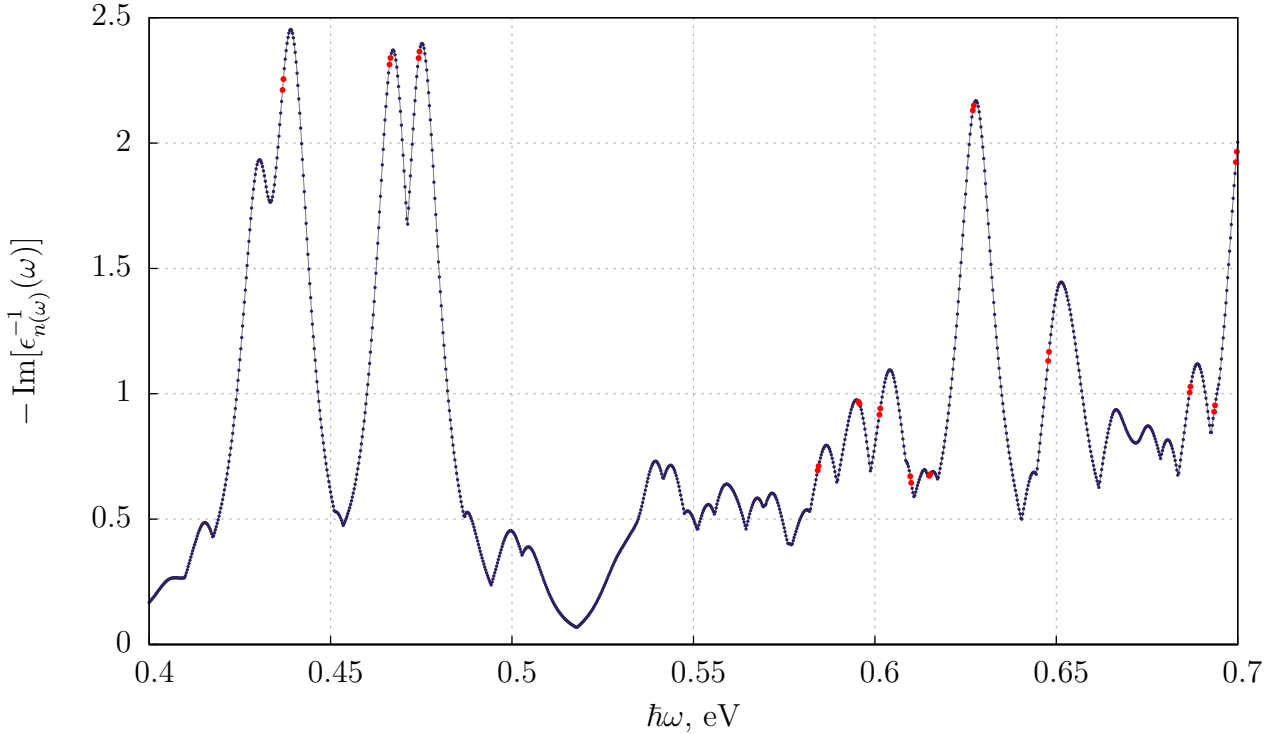


Figure 9: Loss function spectrum with “classical” plasmons marked in red. Each pair of dots indicates a range where the real part of the dielectric function switches sign.

We see that “classical” plasmon frequencies are indeed located near maxima of the loss function. As noted by [Andersen et al., 2012], it’s not important that the peaks do not coincide

<sup>9</sup>

$$\begin{aligned} -\text{Im}[\epsilon(\omega)^{-1}] &= -\text{Im} \left[ \left( 1 - \frac{A}{B - \omega + i \cdot C} \right)^{-1} \right] = -\text{Im} \left[ \frac{B - \omega + i \cdot C}{B - A - \omega + i \cdot C} \right] \\ &= -\text{Im} \left[ \frac{(B - \omega + i \cdot C)(B - A - \omega - i \cdot C)}{(B - A - \omega)^2 + C^2} \right] = -\frac{-C(B - \omega) + C(B - A - \omega)}{(B - A - \omega)^2 + C^2} \\ &= \frac{CA}{(B - A - \omega)^2 + C^2}. \end{aligned}$$

with roots of  $\text{Re}[\epsilon_{n(\omega)}(\omega)]$  as long as the eigenstates  $|\phi_{n(\omega)}(\omega)\rangle$  do not vary much. We can verify this by calculating  $|\langle\phi_{n(\omega_i)}(\omega_i)|\phi_{n(\omega_{i+1})}(\omega_{i+1})\rangle|$ , where  $\omega_i$ 's denote frequencies for which we have calculated  $\hat{\varepsilon}$ . It turns out that except for the points where we “step over” from one peak to another,  $|\langle\phi_{n(\omega_i)}(\omega_i)|\phi_{n(\omega_{i+1})}(\omega_{i+1})\rangle| \approx 1$  with variations of order 1%. This means that to know how plasmon eigenmodes look like, we do need to know neither the precise location of the maximum of  $-\text{Im}[\epsilon_{n(\omega)}^{-1}(\omega)]$  nor the root of  $\text{Re}[\epsilon_{n(\omega)}(\omega)]$ . Knowledge that we are on a particular peak suffices.

As an example, fig. 7 and 8 show  $\text{Re}[\langle\mathbf{r}|\phi_{n(\omega)}(\omega)\rangle]$  for two high peaks at around 0.467 eV and 0.475 eV.

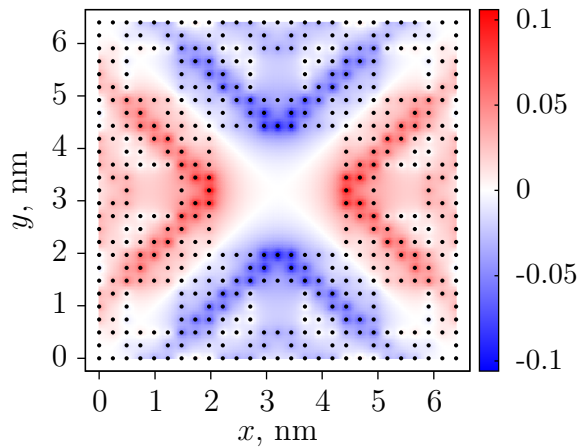


Figure 10: Plasmon eigenmode at frequency corresponding to  $\hbar\omega = 0.46625$  eV

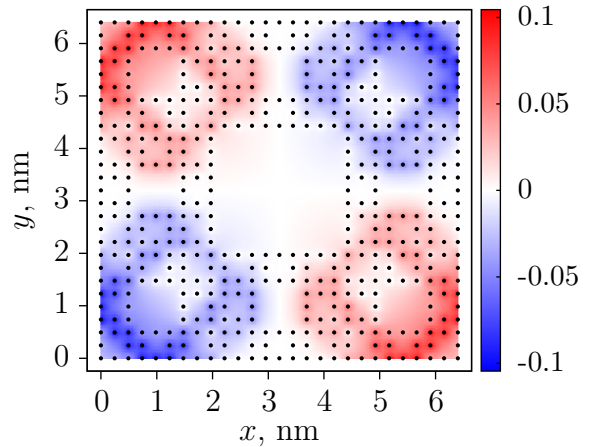


Figure 11: Plasmon eigenmode at frequency corresponding to  $\hbar\omega = 0.47425$  eV

## References

- [Andersen et al., 2012] Andersen, K., Jacobsen, K. W., and Thygesen, K. S. (2012). Spatially resolved quantum plasmon modes in metallic nano-films from first-principles. *Physical Review B*, 86(24):245129.
- [Egerton, 2009] Egerton, R. (2009). Electron energy-loss spectroscopy in the TEM. *Reports on Progress in Physics*, 72(1):016502.
- [Giuliani and Vignale, 2005] Giuliani, G. and Vignale, G. (2005). *Quantum Theory of the Electron Liquid*. Masters Series in Physics and Astronomy. Cambridge University Press.
- [Jackson, 1925] Jackson, J. D. (1925). *Classical Electrodynamics*. John Wiley & Sons, Inc.
- [Nussenzveig, 1972] Nussenzveig, H. (1972). *Causality and Dispersion Relations*. Mathematics in Science and Engineering. Elsevier Science.
- [Vonsovskii and Katsnel'son, 1989] Vonsovskii, S. V. and Katsnel'son, M. I. (1989). *Quantum solid-state physics*, volume 73. Springer Verlag.
- [Wang Weihua et al., 2015] Wang Weihua, Christensen Thomas, Jauho Antti-Pekka, Thygesen Kristian S., Wubs Martijn, and Mortensen N. Asger (2015). Plasmonic eigenmodes in individual and bow-tie graphene nanotriangles. *Scientific Reports*, 5:9535.